Nanostructure of granular Co-SiO_2 thin films modified by thermal treatment and its relationship with the giant Hall effect

Leandro M. Socolovsky,[1,*] Cristiano L. P. Oliveira,[2,3] Juliano C. Denardin,[1] Marcelo Knobel,[1] and Iris L. Torriani[2,3]
[1]*Laboratório de Materiais e Baixas Temperaturas, Instituto de Física "Gleb Wataghin," Universidade Estadual de Campinas, Caixa Postal 6165, 13083-970 Campinas (SP), Brazil*
[2]*Grupo de Cristalografia Aplicada e Raios X, Instituto de Física "Gleb Wataghin," Universidade Estadual de Campinas, Caixa Postal 6165, 13083-970 Campinas (SP), Brazil*
[3]*Laboratório Nacional de Luz Síncrotron, 13084-971 Campinas (SP), Brazil*
(Received 31 March 2005; revised manuscript received 11 August 2005; published 18 November 2005)

Granular cosputtered $Co_{52}(SiO_2)_{48}$ thin films were thermally treated at different temperatures and their magnetotransport and structural properties were investigated. Hall resistivity increases with annealing temperature (T_a), up to T_a=250 °C, and then decreases to a minimum for T_a=400 °C. The structural analysis was based on small-angle x-ray scattering results. A model of a polydisperse system of hard spheres was used to retrieve structural parameters. Results reveal that a volume fraction of Co atoms (approximately 25%) are forming nanospheres. The giant Hall effect depends on a particular combination of nanoparticle diameter, size distribution, and interparticle distance.

DOI: 10.1103/PhysRevB.72.184423 PACS number(s): 78.70.Ck, 75.50.Tt, 73.63.Bd

I. INTRODUCTION

Nanostructured magnetic materials have attracted a great deal of attention in recent decades owing to their intrinsic scientific interest and their potential in technological applications.[1] Magnetic and magnetotransport properties are different from their bulk counterparts when typical sizes are of the order of nanometers. Although not fully understood, properties exhibited by nanostructured materials such as giant magnetoresistance (GMR) and giant Hall effect (GHE) are being intensively studied with the aim of enhancing the properties that make them suitable for information storage technology.[2]

In ferromagnetic materials, the Hall effect has two contributions: ordinary, which appears as a consequence of the Lorentz force; and extraordinary, which is due to the spin-orbit interaction (skew scattering and/or side jump).[3] In normal metals, the extraordinary contribution is small.[3] In cermet-type materials, both contributions (ordinary and extraordinary) show large values near the percolation threshold, and this phenomenon has been known as the giant Hall effect.[4] Although GHE in nonmagnetic granular systems has been accounted for with relative success within the local quantum interference model,[5] the understanding in magnetic systems is far from complete. Some ideas to explain this effect have been presented, but a full picture is still missing.[6,7] A mechanism of boundary scattering was considered to develop and support a model for GHE.[8]

Generally speaking, it is widely accepted that magnetotransport properties of granular systems arise as a consequence of their nanostructure. Existence of nanosized clusters is a condition for the appearance of both GMR and GHE in granular systems.[6,9] To develop a model for GHE, it is necessary to obtain a reliable structural characterization of the particle system. Transmission electron microscopy (TEM) techniques present inherent difficulties in the case of concentrated systems because the micrographs obtained represent projections of a three-dimensional system onto a plane. In addition, the statistics of the histograms is poor due the limited particle count, generally limited to a few thousand particles in a typical area of 10^{-7} mm^2. On the other hand, small-angle x-ray scattering (SAXS) can provide values that represent the scattering of a large number of particles ($\sim 10^{16}/mm^3$). SAXS samples do not require specific treatment for the measurements, while in TEM experiments small changes can be induced because of sample preparation (polishing, dimpling, ion bombardment),

To gain insight into the relationship between nanostructure and the giant Hall effect, we prepared several thin films of cobalt and SiO_2 by cosputtering, varying Co concentration x from 25 to 100 vol %. The changes in the nanostructure induced by thermal treatment were studied performing SAXS and wide-angle x-ray scattering (WAXS) experiments. A discussion is presented on how the granular morphology affects the extraordinary Hall resistivity.

II. EXPERIMENTAL DETAILS

Co-SiO_2 films made by cosputtering were produced by magnetron cosputtering at the Physics Department of the Hong Kong University of Science and Technology (PD—HKUST). Films were deposited on glass and kapton substrates. The substrate was kept at room temperature during the process. Pressure before sputtering was 10^{-7} Torr and during the process it was kept at 5 mTorr, the chamber filled with Ar. The substrates were rotated during sputtering to ensure composition uniformity. The Co volume fraction was controlled by the relative sputtering rates, and subsequently confirmed by energy-dispersive x-ray spectroscopy using a Philips EDAX XL30 device. We chose the sample that showed the highest GHE (x=52 vol %)[2] and thermally treated it at different temperatures T_a=150, 200, 250, 300, 350, and 400 °C. Annealing was done in a sealed oven, in a vacuum better than 2×10^{-6} Torr. Thermal treatment was

 ©2005 The American Physical Society

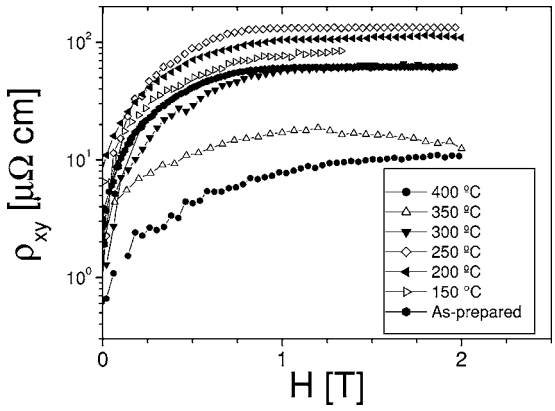

FIG. 1. Hall resistivity measurements for $Co_{52}(SiO_2)_{48}$ samples thermally treated at different temperatures, measured at room temperature.

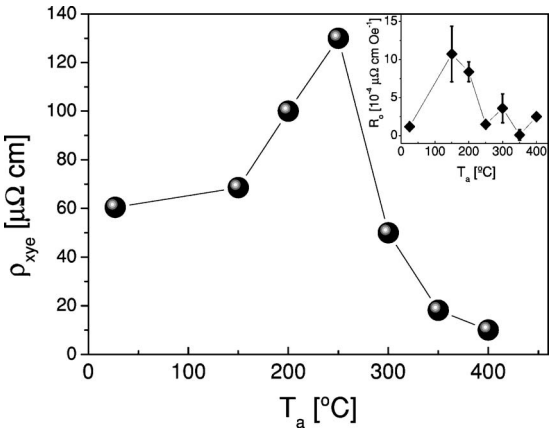

FIG. 2. Extraordinary Hall resistivity vs annealing temperature T_a, measured at room temperature. A maximum is seen at $T_a = 250$ °C. In the inset: ordinary Hall coefficient R_o vs T_a.

done using a fast heating rate, up to the desired temperature, then keeping the temperature constant for 15 min and subsequently turning off the heating power, as a way to fast cool the samples without exposing them to contaminants or air.

Samples prepared for SAXS/WAXS measurements were deposited on kapton films in the same run together with those to be used in the Hall effect measurements. SAXS and WAXS experiments were performed at the SAS beamline of the National Synchrotron Light Laboratory (LNLS, Campinas, Brazil).[10] Transmission mode was used, with a wavelength of $\lambda = 1.756$ Å. A camera length of 60 cm allowed us to measure SAXS intensity in a scattering vector range of $0.01291 \leqslant q \leqslant 0.40$ Å^{-1}. WAXS images were obtained with an image plate. Transmission electron microscopy was performed with a Jeol JEM-3010 ARP microscope operating at 300 KV (resolution 1.7 Å), at the LME (LNLS). Magnetic measurements were performed with a Quantum Design MPMS XL7 SQUID magnetometer. Magnetotransport properties were measured at room temperature with conventional four-contact geometry, for fields up to 2 T.

III. RESULTS AND DISCUSSION

Hall resistivity ρ_{xy}, shown in Fig. 1, clearly changes with annealing temperature. Extraordinary Hall resistivity is extracted from the extrapolation of the saturated value of ρ_{xy} to $H = 0$. It increases, from a value of 60.5 $\mu\Omega$ cm for the as-prepared sample up to 250 $\mu\Omega$ cm for a sample annealed at 250 °C, and then decreases down to 11 $\mu\Omega$ cm for T_a

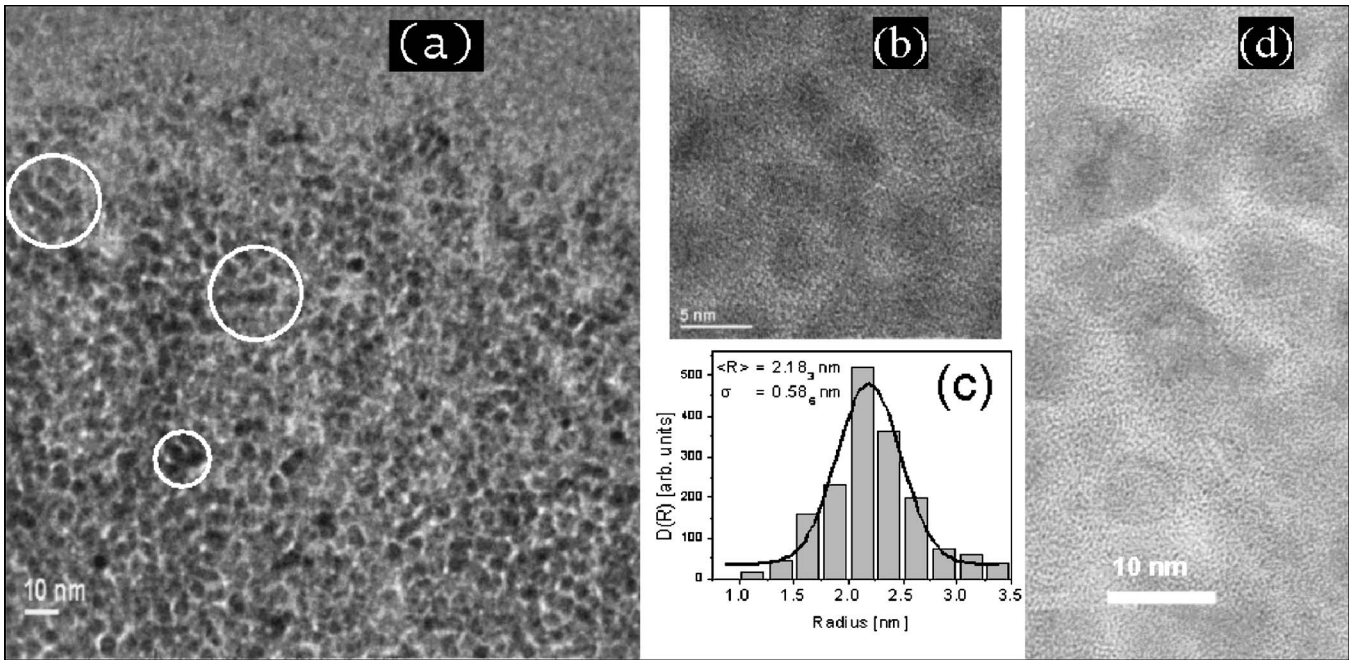

FIG. 3. TEM images of the sample annealed at $T_a = 250$ °C [(a) and (b)] and 400 °C (d). A particle volume distribution histogram (c) created by carefully measuring each distinguishable particle size (a Gaussian distribution was fit). High-resolution images show nanoparticles in close contact [(b) and (d)]. The circles indicate several aggregated particles.

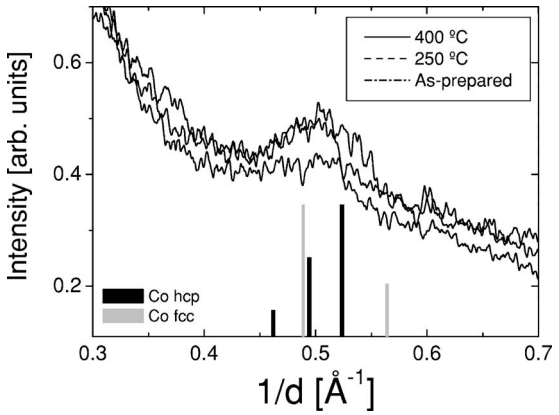

FIG. 4. Wide-angle x-ray scattering obtained for the samples as-prepared and treated at 250 and 400 °C. Peak positions and relative intensities for fcc-Co and hcp-Co are indicated as vertical bars.

$=400$ °C as seen in Fig. 2. The ordinary Hall coefficient R_o was calculated as the slope of the saturated part of the ρ_{xy} curve. R_o increased from 1.2×10^{-4} $\mu\Omega$ cm/Oe (as prepared) up to 10×10^{-4} $\mu\Omega$ cm/Oe ($T_a=150$ °C), and then fell down to values between 0.8 and 3.6×10^{-4} $\mu\Omega$ cm/Oe for $T_a\geqslant250$ °C (inset of Fig. 2). A similar behavior was observed in NiFe-SiO_2 samples,[6] in which GHE increased up to $T_a=300$ °C, and diminished with further annealing.

TEM images (Fig. 3) showed that the system was composed of nanoparticles. From the particle size distribution histogram, a particle volume distribution was created for the sample annealed at 250 °C [Fig. 3(c)]. A Gaussian approximation yielded values of mean radius $\langle R\rangle=2.19\pm0.03$ nm, and $\sigma\approx0.5$ nm for the NPs.

The WAXS measurements are shown in Fig. 4. They display a diffuse background characteristic of an amorphous phase, and a broad peak located at $q\sim0.5$ Å^{-1}, which may correspond either to hcp-Co, fcc-Co, or a mixture of both phases. SAXS spectra (Fig. 5) showed features typical of polydisperse systems. For very low values of q, the curves exhibited a sharp rise, as seen in the insets of Fig. 5, attributed to the presence of very large particles. A maximum located at $q=0.1-0.2$Å^{-1} indicates the existence of spatial correlation effects deriving from nanoparticle interaction. Due to the high volume fraction of nanoparticles in the sample, structure factor effects become relevant for the analysis of the scattering data.[11]

A model that describes SAXS intensities and takes into account particle form factor, system structure factor, particle size distribution, and volumetric fraction was used to analyze the measured spectra. The following expression was employed:[11,12]

$$I(q)=\text{const}\, I_0(q,\langle R\rangle,\sigma)S(q,R_{\mathrm{HS}},\eta), \tag{1}$$

where we have the following:

(i) $I_0(q,\langle R\rangle,\sigma)=\int_0^\infty D(R)V(R)\Delta\rho(R)^2P(q,R)dR$ is the scattering intensity (particles without interaction) of the polydisperse system, with $D(R)$ the volume distribution function (center $\langle R\rangle$, width σ), $V(R)$ is the particle volume, $\Delta\rho(R)$ is the electronic density contrast, and $P(q,R)$ is the normalized particle form factor of the particles with size R (in our case, spheres). A Gaussian distribution was assumed for the particle volume distribution.

(ii) $S(q,R_{\mathrm{HS}},\eta)$ is the structure factor, calculated using the Percus-Yevick[11] approximation for hard-sphere interaction, with R_{HS} the hard-sphere interaction radius and η the hard-sphere volume fraction.

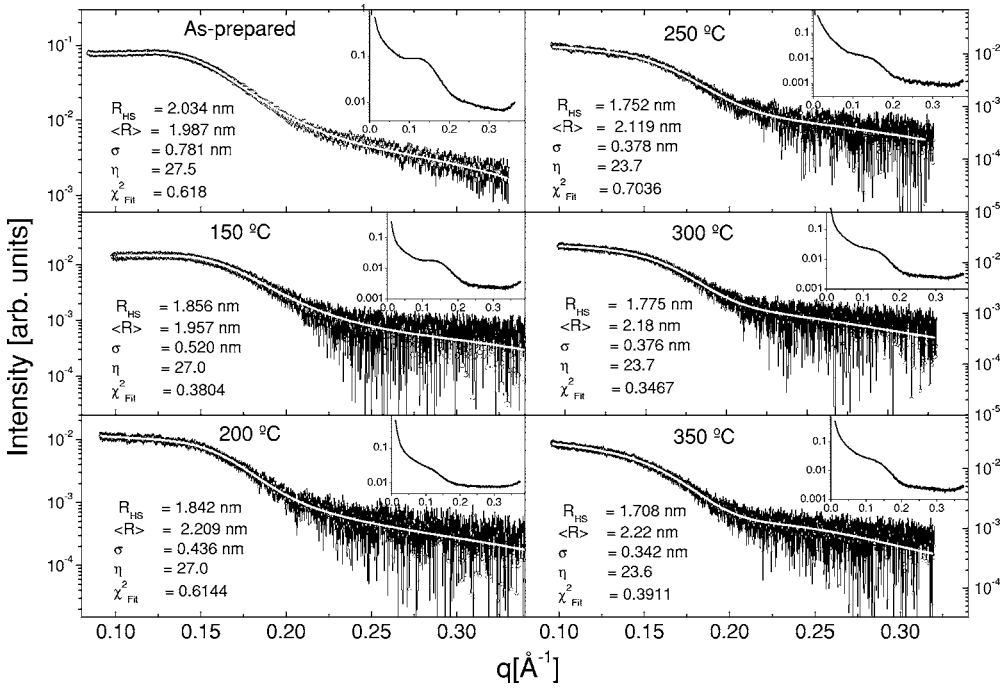

FIG. 5. Small-angle scattering measurements (points with error bars) and fit (white line) of the region of interest, T_a. Fitting parameters are included in the plot. In the insets: corresponding full-range spectrum.

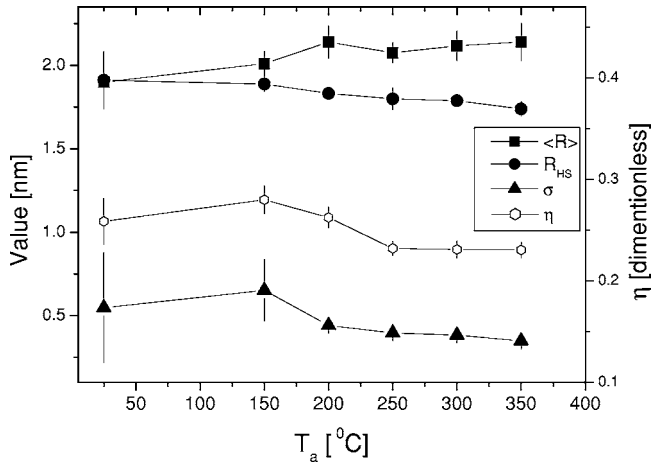

FIG. 6. Structural parameters vs annealing temperature. A stationary value is reached for $\langle R\rangle$, and decreasing σ with increasing T_a indicate that smaller particles are coalescing or incorporating into the bigger ones. The evolution of the volumetric fraction η (open diamonds) suggests that part of the nanoparticles coalesce into larger structures.

A fitting routine developed by Svergun *et al.*[12] was used for the calculations. Satisfactory curve fittings could be obtained only when the contribution of large particles at very low q was subtracted from the scattering signal. Following this procedure, fittings were quite good in all cases, as can be seen in Fig. 5. Several fittings were performed for each spectrum using different values of η. The best value of η was taken from the fit that minimized the discrepancy (χ) between the calculated intensity and the experimental data. Surprisingly, the value of η that minimized χ for all samples (even those with higher cobalt concentration) was around 25%, thus indicating that this volume fraction corresponds to the maximum amount of cobalt atoms forming the main population of interacting spherical particles in the granular system. The extra Co atoms present in the samples with higher concentrations may contribute to the formation of very large clusters, whose presence is considered to be responsible for the sharp rise of the intensity values in the small-q region. Fitting parameters are plotted against thermal treatment temperature T_a in Fig. 6. It can be seen that when T_a increases, $\langle R\rangle$ increases, and σ decreases up to $T_a = 250\,^{\circ}\mathrm{C}$ when both values stabilize. Also, R_{HS} decreases monotonically. Note that η varies between 26 and 28% (taking into account the error bar) for $T_a \leqslant 200\,^{\circ}\mathrm{C}$, and falls down to $\sim$23% for higher annealing temperatures, indicating that some nanoparticles are forming larger structures. It should be emphasized that in a system of interacting particles like the one we are considering, the scattering intensity is described by Eq. (1). R_{HS} variations (related to interparticle distances) are accounted for by the structure factor $S(q)$, and the mean particle radii $\langle R\rangle$ depend on the particle form factor $P(q)$. Consequently, it is clear that aggregation (fusing) processes are expected to lead to decreasing R_{HS} values and the form factor of fused particles will lead to larger values of $\langle R\rangle$.

To support the idea of particles coalescence, zero-field-cooling magnetization measurements were performed (Fig. 7). The ZFC curves are typical of a system of nanoparticles with a superparamagnetic-like peak, which shifts to higher temperatures with annealing (see Fig. 7). This is indicative of increasing particle size and/or magnetic interactions among nanoparticles.[13,14]

The sputtering process produces a variety of granular systems: amorphous large structures, nanoparticles, and isolated atoms. The explanation for the observed changes in the Hall resistivity with the thermal treatment can be based on the subtle variations of the structural parameters and the interplay between these structures. The physical meaning of an R_{HS} value lower than $\langle R\rangle$ is that the particles may be in close contact. Decrease of the R_{HS} value with T_a can be due to an increasing number of agglomerated or partially fused particles. As mentioned before, the mechanisms for the giant Hall effect are still unclear for magnetic systems. Two connected NPs could create a source for GHE due to surface roughness, tiny conductive channels, or point contacts.[5,9,15,16]

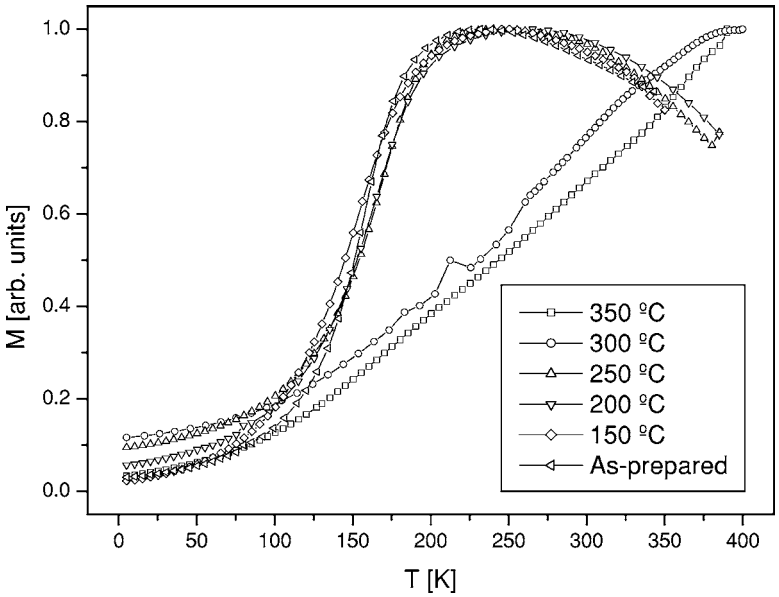

FIG. 7. Zero-field-cooling magnetization for all the samples. Above $T_a = 250\,^{\circ}\mathrm{C}$, the curves remain unchanged. For higher temperatures, the maximum shifts to bigger values: ZFC measurement for the sample annealed at 300 °C has a maximum at $T = 396$ K. For the sample treated at 350 °C, it peaks at $T \approx 473$ K. This fact indicates increasing NP size and/or increasing interactions.

Analyzing the Hall effect measurements with the structural data in mind, one can separate the process into four different stages. For as-prepared samples, the conduction of the electrons is done through conduction channels between nanoparticles. These channels could be chains of isolated atoms and/or the tiniest NP. For $T_a < 200$ °C, thermal treatment increases the nanoparticle mean radius $\langle R \rangle$, but the size distributions σ and η experience no changes; so the minute channels disappear (part of these atoms incorporating into the NPs), thus increasing the ordinary and extraordinary Hall resistivity. For $T_a = 200$ and 250 °C, NPs reach their maximum mean size, and the size distribution σ shrinks, leaving fewer channels for the conduction electron hopping, thus increasing the Hall resistivity. Considering the decreasing R_{HS} values, we can picture at this point that the main source for GHE is the contact region between adjacent NPs. For $T_a > 250$ °C, the situation is almost the same, but taking into account that R_{HS} is lower than before, the samples exhibit more and larger channels for conduction electrons through the contact points between NPs, leading to a normal conduction through the NPs, and therefore decreasing the Hall resistivity.

The results of the SAXS measurements gave new insight into the granular structure of the system. A combined analysis of the experiments showed that the giant Hall effect appears as a particular combination of mean particle radius $\langle R \rangle$, size distribution width σ, and hard-sphere radius R_{HS}. SAXS measurements have proven to be a reliable technique to measure small-scale structural changes in these concentrated systems. More experiments are being performed in similar systems in search of general features that could clearly establish the relationship between nanostructure and extraordinary Hall effect.

ACKNOWLEDGMENTS

We acknowledge the Brazilian agencies Fundação de Amparo à Pesquisa do Estado de São Paulo (FAPESP), Conselho Nacional de Desenvolvimento Científico e Tecnológico (CNPq), and Synchrotron Light National Laboratory (LNLS, Campinas, Brazil—Projects SAS 1138 and 1536, and LME for the use of TEM) for support. Thanks are also due to Professor Dr. X. X. Zhang (PD-HKUST) for sample preparation.

*Author to whom correspondence should be addressed. Email address: leandros@ifi.unicamp.br

[1] X. Battle and A. Labarta, J. Phys. D **35**, R15 (2002).
[2] J. C. Denardin, M. Knobel, X. X. Zhang, and A. B. Pakhomov, J. Magn. Magn. Mater. **262**, 15 (2003).
[3] C. M. Hurd, *The Hall Effect in Metals and Alloys* (Plenum, New York, 1972).
[4] A. B. Pakhomov, X. Yan, and B. Zhao, Appl. Phys. Lett. **67**, 3497 (1995).
[5] X. X. Zhang, C. Wan, H. Liu, Z. Q. Li, P. Sheng, and J. J. Lin, Phys. Rev. Lett. **86**, 5562 (2001).
[6] X. N. Jing, N. Wang, A. B. Pakhomov, K. K. Fung, and X. Yan, Phys. Rev. B **53**, 14032 (1996).
[7] A. B. Pakhomov, X. Yan, N. Wang, X. N. Jing, B. Zhao, K. K. Fung, J. Xhie, T. F. Hung, and S. K. Wong, Physica A **241**, 344 (1997).
[8] F. Brouers, A. Granovsky, A. Sarychev, and A. Kalitsov, Physica A **241**, 284 (1997).
[9] C. L. Chien, J. Q. Xiao, and J. S. Jiang, J. Appl. Phys. **73**, 5309 (1993).
[10] G. Kellerman, F. Vicentin, E. Tamura, M. Rocha, H. Tolentino, L. Barbosa, A. Craievich, and I. Torriani, J. Appl. Crystallogr. **30**, 1 (1997).
[11] C. Robertus, W. H. Philipse, J. G. H. Joosten, and Y. K. Levine, J. Chem. Phys. **90**, 4482 (1989).
[12] D. I. Svergun, P. V. Konarev, V. V. Volkov, M. H. J. Koch, W. F. C. Sager, J. Smeets, and E. M. Blokhuis, J. Chem. Phys. **113**, 1651 (2000).
[13] J. M. Vargas, L. M. Socolovsky, M. Knobel, and D. Zanchet, Nanotechnology **16**, S285 (2005).
[14] M. Knobel, W. C. Nunes, A. L. Brandl, J. M. Vargas, L. M. Socolovsky, and D. Zanchet, Physica B **354**, 80 (2004).
[15] B. A. Aronzon, V. V. Rylkov, D. Yu. Kovalev, E. Z. Meilikhov, A. N. Lagarkov, M. A. Sedova, M. Goiran, N. Negre, B. Raquet, and J. Leotin, Phys. Status Solidi B **218**, 169 (2000).
[16] A. Gerber, A. Milner, A. Finkler, M. Karpovski, L. Goldsmith, J. Tuaillon-Combes, O. Boisron, P. Mélinon, and A. Perez, Phys. Rev. B **69**, 224403 (2004).